

## Ultra low loss and dual polarized SPR-PCF sensor based on refractive index

Dedi Irawan<sup>1</sup>, Khaikal Ramadhan<sup>2</sup>, Saktioto<sup>3</sup>, Fitmawati<sup>4</sup>, Dwi Hanto<sup>5</sup>, Bambang Widiyatmoko<sup>5</sup>,  
Azwir Marwin<sup>3</sup>, Azhar<sup>1</sup>

<sup>1</sup>Laboratory of PMIPA, Department of Physics Education, Universitas Riau, Pekanbaru, Indonesia

<sup>2</sup>Department of Physics, Faculty of Mathematics and Natural Sciences (FMIPA), Institut Teknologi Bandung, Bandung, Indonesia

<sup>3</sup>Department of Physics, Faculty of Mathematics and Natural Sciences (FMIPA), Universitas Riau, Pekanbaru, Indonesia

<sup>4</sup>Department of Biology, Faculty of Mathematics and Natural Sciences (FMIPA), Universitas Riau, Pekanbaru, Indonesia

<sup>5</sup>Research Center for Physics, National Research and Innovation Agency, Puspitek Serpong, Tangerang Selatan, Indonesia

### Article Info

#### Article history:

Received Jun 21, 2022

Revised Jul 14, 2023

Accepted Jul 30, 2023

#### Keywords:

Photonics crystal

Refractive index

Surface plasmon resonance

Ultra-sensitivity

### ABSTRACT

In this paper presents a numerical simulation using the finite element method (FEM) to analyze the performance of a photonic crystal fiber (PCF) integrated with plasmonic material sensor components. The sensor comprises silica and Au layers with a thickness of 45 nm, arranged in a simple geometric structure. Our proposed sensor component exhibits ultra-low loss, distinguishing it from previous studies that have focused on wavelength-sensitive (WS) and amplitude-sensitive (AS) measurement techniques. The refractive index (RI) range of the sensor component spans from 1.32 to 1.38 RIU. The maximum WS and AS values achieved are 6,000 nm/RIU, -373.4 1/RIU (x-polarization), and -385.4 1/RIU (y-polarization), respectively. Moreover, we demonstrate an ultra-low loss of 0.00117 dB/cm (x-polarized) and 0.00307 dB/cm (y-polarized). In terms of sensor resolution, this design achieves a remarkable resolution of  $1.6 \times 10^{-7}$  RIU for both x-and y-polarized measurements.

*This is an open access article under the [CC BY-SA](#) license.*



### Corresponding Author:

Dedi Irawan

Laboratory of PMIPA, Department of Physics Education, Universitas Riau

Pekanbaru, Indonesia

Email: [dedi.irawan@lecturer.unri.ac.id](mailto:dedi.irawan@lecturer.unri.ac.id)

## 1. INTRODUCTION

The need for optical sensors continues to increase, this is due to the extraordinary capabilities of optical sensors such as high sensitivity wide sensing range, resistance to electromagnetic wave interference, and very small size [1], so it can be designed with a portable size and working based on wavelength. Several optical sensors have reached the commercialization process while some are still in the development stage, various types of optical based sensors including optical fiber, multi-mode fiber, fiber Bragg grating (FBG) [2], [3], tapered FBG, and optical fiber based surface plasmon resonance-photonic crystal fiber (SPR-PCF) [4], [5]. Also, several sensing techniques have been reported by many researchers, including the Mach Zehnder interferometer technique. Optical-based recently, the combination of SPR-PCF has given rise to technologies, the component is widely used in many fields, such as temperature sensors, refractive index (RI), strain, magnetic field (MF), and biological samples [6]. Not only that, various studies have reported, this component can measure more than one physical quantity simultaneously like measuring temperature and RI simultaneously, RI and MF simultaneously, and temperature and RI simultaneously [7]–[9].

SPR-PCF components have been widely developed by many researchers, some components are reported to have ultra-sensitivity, easy to fabricate, simple structure, and multi-function capabilities. Researchers also have developed various sensor component geometric structures, such as the SPR-PCF with a

D-shaped structure [10], octagonal, and hexagonal [11]. Air holes are also engineered by making circle-shaped holes, square-shaped holes, and rectangular-shaped holes. Recently, massive numerical engineering has been carried out in integrating sensor building materials, such as engineering dielectric materials using ZEONEX, topaz, silica, as well as engineering plasmonic materials to generate surface plasmon resonance (SPR) phenomena using gold and silver [12], [13].

Low loss is very important in sensor capabilities and this factor is a challenge in fabricating sensor components, low loss will provide a low signal loss capability to the component. Mahfuz *et al.* [14] proposed SPR-PCF sensor component capable of sensing in the RI range 1.32 to 1.4 RIU and it was reported that the sensor has a minimum low loss of 0.22 dB/cm, while the sensor he proposed is composed of fused silica,  $\text{TiO}_2$ , and gold materials layers. Islam *et al.* [15] reported work for the SPR-PCF component which has dual-polarized propagation. The sensor components are fused silica,  $\text{TiO}_2$ , and gold coating [15]. Yang *et al.* [16] also reported their work related to the SPR-PCF component in detecting kerosene concentrations in the concentration range of 0% to 90%, in their work obtaining a confinement loss (CL) of 5.4 dB/cm. Nuzhat *et al.* [17] reported ultra-sensitivity SPR-PCF sensor components in detecting the analyte RI, the detection ranges from 1.33 to 1.4 RIU. The sensor component is reported to have the dual-polarized capability with a maximum CL of 10.71 dB/cm (x-polarized) and 28.58 dB/cm (y-polarized), the amplitude-sensitive (AS) sensing technique is also introduced here and the AS is -1,212 1/RIU (x-polarized) and -2430 1/RIU (y-polarized), the sensor material consists only of silica and a layer of gold [17]. Sultana *et al.* [18] also studied the photonic crystal fiber (PCF) materials used were  $\text{TiO}_2$ , gold, and fused silica. Meanwhile AS sensing technique was also introduced and obtained 2,561 1/RIU and figure of merit (FOM) 118.75 1/RIU. In this study, we investigation of SPR-PCF with simple geometric structure (three types of air hole with different sizes) which has a low-loss propagation and it works on dual-polarized. In this structure we build with fused silica and gold materials, the gold layer is chemically stable.

## 2. STRUCTURE DESIGN AND NUMERICAL ANALYSIS

Figure 1 display the structure geometry of sensor component with twelve large air holes with diameter  $d_3=d/4$ , then 12 medium-sized holes  $d_2=d/2.5$ , and two small air holes with size  $d_1=d/2$  with value of  $d=1.6 \mu\text{m}$  which is close to the sensor core. The next layer is plasmonic material attached to the sensor, so this sensor is included in external sensing with a layer thickness of 45 nm. The hole sizes will be varied to  $0.4 \mu\text{m}$ ,  $0.45 \mu\text{m}$ , and  $0.5 \mu\text{m}$  based on the CL. The thickness of the analyte layer is  $0.5 \mu\text{m}$  which lies after the gold layer. The last layer in this numerical simulation is perfectly matched layer (PML) with a thickness of  $1 \mu\text{m}$ . the distance between  $d_1$  and  $d_2$  air holes is  $2.1 \times p$ , and the distance between  $d_2$  and  $d_3$  holes is  $3 \times p$ , where the value of  $p=1.7 \mu\text{m}$  the RI of the analyte varies from 1.32 to 1.38 RIU, the gold layer being the most sensitive layer due to the SPR phenomenon. Investigations carried out using the finite element (FE), we use the element mesh is normal, so it can provide high accuracy for each element that is traversed by electromagnetic waves [19]–[21]. In sensing, the SPR-PCF sensor has a simple label-free system as shown in Figure 2. The FE method applied sensor component is used to investigate the propagation mode of the material using maxwell's equations. With  $\varphi$  represent the MF and electric field (EF), relative permittivity and capability tensor represented by [l] and [m] which can be defined by (1) and (2):

$$[m] = \begin{bmatrix} m_x & 0 & 0 \\ 0 & m_y & 0 \\ 0 & 0 & m_z \end{bmatrix} \quad (1)$$

$$[l] = \begin{bmatrix} l_x & 0 & 0 \\ 0 & l_y & 0 \\ 0 & 0 & l_z \end{bmatrix} \quad (2)$$

Where  $m_x = m_y = m_z = 1$ ,  $l_x = n_x^2$ ,  $l_y = n_y^2$ ,  $l_z = n_z^2$  for the EF with  $\varphi = E$  and  $l_x = l_y = l_z = 1$ ,  $m_x = \frac{1}{n_x^2}$ ,  $m_y = \frac{1}{n_y^2}$ ,  $m_z = \frac{1}{n_z^2}$  for a MF with  $\varphi = H$  provided that  $n_x, n_y, n_z$  are not a Boundaries, but additional layers that absorb radiation. If we assume that PML is a parallel coordinate plane with matrix forms which can be defined by (3):

$$[s] = \begin{bmatrix} \frac{s_y s_z}{s_x} & 0 & 0 \\ 0 & \frac{s_x s_z}{s_y} & 0 \\ 0 & 0 & \frac{s_y s_x}{s_z} \end{bmatrix} \quad (3)$$

The matrix in (3) can be modified with Maxwell's as in (4):

$$\nabla \times ([l][s]^{-1} \nabla \times \varphi) - k_0^2 [m][s] \varphi = 0 \quad (4)$$

Where  $s_x, s_y, s_z$  are scaling parameters that have complex values. This parameter can have a value of alpha, leaky mode analysis can be assumed  $\alpha = 1 - \alpha_j$  with value  $i \alpha_j$  can show the scenario of absorption and no absorption which can be written by (5):

$$\alpha_j = \alpha_j \max \left( \frac{\rho}{\omega} \right)^2 \quad (5)$$

Where  $\omega$  represent the thickness of the PML layer and  $\rho$  represent of the distance from the start of the PML. As shown in Figure 1, this sensor component is composed of  $\text{SiO}_2$  material in the core, RI distributions depends on the wavelength. COMSOL-based FE is used in investigating the performance of sensor components, in COMSOL we define fused silica material using the Sellmeier as in (6). Meanwhile, the values for each symbol in (6)  $A1=0.696163$ ,  $A2=0.4079426$ ,  $A3=0.897479400$ ,  $B1=0.0046791486 \mu\text{m}^2$ ,  $B2=0.0135120631 \mu\text{m}^2$ ,  $B3=97.9340025 \mu\text{m}^2$ .

$$n(\lambda) = \sqrt{1 + \frac{A1\lambda^2}{\lambda^2-B1} + \frac{A2\lambda^2}{\lambda^2-B2} + \frac{A3\lambda^2}{\lambda^2-B3}} \quad (6)$$

Where  $n$  represent the RI of  $\text{SiO}_2$  depend on wavelength,  $\lambda$  represent the wavelength, and the value of each variable are accordance to [22] while the gold material can be defined by the Drude-Lorentz model equation which is written in (7) and the value of each variable can be seen in [23]:

$$\varepsilon_{au} = \varepsilon_{\infty} - \frac{\omega_D^2}{\omega(\omega+j\gamma_D)} - \frac{\Delta\varepsilon\Omega_L^2}{(\omega^2-\Omega_L^2)+j\Gamma_L\omega} \quad (7)$$

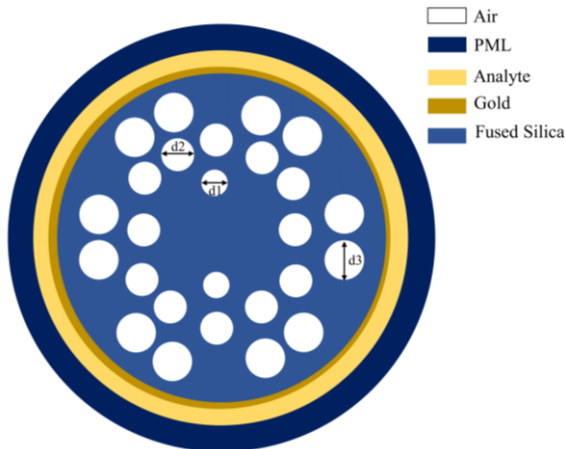


Figure 1. Sensor geometry structures

### 3. RESULTS AND DISCUSSION

Electrical distribution result related to CL sensor. In this paper we introduce dual polarization of SPR-PCF, each polarization on the x-axis and y-axis on the cross section can be used to detect analytes, that is based on 2D component sensor. For electrical distribution x-polarized on the core can be seen in Figure 2(a) and for y-polarized in Figure 2(b). The CL of the sensor can be calculated using (8). Where CL represent the CL of the PCF, frequency, effective RI, speed of light represents with  $f$ ,  $n_{eff}$ , and  $c$ .

$$C_L(\text{dB/cm}) = \left( \frac{4\pi f}{c} \right) \text{Im}(n_{eff}) \times 10^4 \quad (8)$$

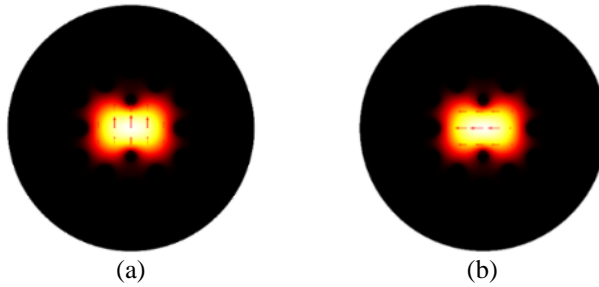


Figure 2. The EF distribution on the SPR-PCF cross-section; (a) y-polarized and (b) x-polarized

### 3.1. Dual-polarized sensitivity analysis

The initial part of the numerical simulation is to engineer the geometric structure of the sensor, after structural engineering is carried out, work continues to define the constituent materials of each designed geometric structure, such as defining the RI of air holes, defining RI of  $\text{SiO}_2$  material using (6), and the last is to define plasmonic material (gold). After the design and material have been defined in COMSOL multiphysics, a mode analysis of the design is performed with the ultimate goal of obtaining the imaginary effective RI for each wavelength. Obtain the CL of the design from the imaginary numbers using (8). Therefore, surface plasmon waves (SPW) can occur when the frequency of the wavelength around the conductive core is the same as the frequency or wavelength of the surface electrons. SPW is very sensitive to surface RI [24].

The SPR-PCF sensor components which have been previously reported by many researchers, not all sensor components have dual-polarized propagation performance, some of which only have consistent performance on either x-polarized or y-polarized. Hossain *et al.* [25] only performed on y-polarized this is associated with increased RI mode and high radiation loss when compared to x-polarized, Singh and Prajapati [26] with d-shaped SPR-PCF component found two polarized components, and found y-polarized to be the fundamental mode due to the very large connection and surface plasmon polariton (SPP) mode compared to x-polarized. Several studies also have reported single polarization screening in which one of the polarizations is suppressed and the other is well guided. Dou *et al.* [27] used single-polarized SPR-PCF in describing CL, at wavelengths range from 1,310 nm to 1,550 nm, CL were found to be 244.9 dB/cm and 292.8 dB/cm respectively. It is found that the y-polarized has a larger CL distribution than the x-polarized, and the CL for each x-polarized and y-polarized are 0.019185 dB/cm and 0.048643 dB/cm at a wavelength of 700 nm, for all polarized analysis in Table 1.

Table 1. Polarized analysis

RI (RIU)	CL (dB/cm)	WS (nm/RIU)	RW (nm)	AS (y) (1/RIU)	AS (x) (1/RIU)
1.32	0.003067	-	590	-	-
1.33	0.004553	1000	600	-105.143	-105.9
1.34	0.007301	2000	620	-132.22	-133.2
1.35	0.012359	2000	640	-186.3	-186.6
1.36	0.023643	2000	660	-258.2	-226.1
1.37	0.048643	4000	700	-344.9	-294
1.38	0.124544	6000	760	-385.4	-373.4

### 3.2. Wavelength-sensitivity

Wavelength-sensitive (WS) is an important component in characterizing sensor performance. WS can be calculated using (9):

$$S_\lambda(\text{nm/RIU}) = \Delta\lambda_{\text{peak}}/\Delta n_a \quad (9)$$

Where  $\Delta\lambda_{\text{peak}}$  represent for change in peak wavelength, meanwhile  $\Delta n_a$  is the shift in RI of the two analytes. In the sensor design, the analyte RI from 1.32 to 1.38 RIU. RW range from 590 nm to 760 nm, with variations of 1.32, 1.33, 1.34, 1.35, 1.36, 1.37, and 1.38 RIU. Further shift of the CL peak for each change of RI as shown in Figure 3(a), for y-polarized. SPR-PCF is based on evanescence wave, in this design we introduce dual polarized low loss, the loss on the y-polarized can be seen in Figure 3(b). RI range from 1.32–1.38 RIU, the resonant wavelength shifts with every change in the analyte RI. For the smallest RI 1.32 RIU, wavelength resonance was found at 590 nm, while the sensor material loss was found of 0.003067 dB/cm. The variation of

the analyte RI in this design is 0.01 RIU, so, when the analyte RI is increased to 1.33 RIU, the y-polarized loss of material increases by 0.004553 dB/cm and the RW is found at 600 nm, the WS is 1000 nm/RIU. When analyte RI at 1.34 RIU, the CL also increases namely 0.007301 dB/cm with the RW at 620 nm, in this range of RI it is found that the WS is 2,000 nm/RIU some time, there is an increase in analyte RI always followed by a shift in the RW at y-polarized, the largest increase occurred in the range of RI from 1.37 to 1.38 RIU, in the design it was found that the increase in CL from 0.048643 dB/cm to 0.124544 dB/cm, then a shift in the RW from 700 nm to 7600 nm, so, in this range found that the WS is 6,000 nm/RIU which is also the maximum WS of the proposed sensor design. Further related to the analysis on y polarized in Table 1.

Meanwhile, the RW shift for each index of refraction also occurs in the same way for x-polarized as shown in Figure 3(a). The RW ranges from 590 nm to 760 nm, the difference from the previous x-polarized is the CL for each index analyte bias. At an analyte RI of 1.32 CL of 0.001174861 dB/cm and a RW of 590 nm. In this case the value of CL is smaller than y-polarized, then, when analyte RI is increased to 1.33 RIU, the CL of the sensor component is 0.001743885 dB/cm. There is an increase in CL in this RI range. Similarly, the y-polarized RW is found at 600 nm. In general, the trend of shifting RW in x-polarized is the same as in y-polarized, while there is a difference in CL. If we compare with the proposed sensor components by previous researchers, we show a very small CL value. Zuhayer *et al.* [28] conducted a numerical investigation on the d-shaped twin core sensor design obtained minimum CL at x-polarized and y-polarized of 57.87 dB/cm and 36.54 respectively with an analyte RI of 1.4, meanwhile Shakya *et al.* [1] reported on the sensor design having a minimum CL of 80 dB/cm on x-polarized and y-polarized, Sultana *et al.* [18] obtained a minimum CL in their SPR-PCF sensor design of 0.224 dB/cm for RI 1.27. Nuzhat *et al.* [17] obtained a minimum CL in their sensor design of 0.112 dB/cm for RI 1.33 (x-polarized) and 0.27 dB/cm (y-polarized). Further on the sensor design that we propose for x-polarized can be seen in Table 2. The slope of the curve is an important factor in the average resolution and sensitivity of the sensor. As long as, the change in the analyte RI from 1.32–1.38 RIU with the RW in the range from 590 nm to 760 nm. At analyte RI of 1.32, 1.33, 1.34, 1.35, 1.36, 1.37, and 1.38, resonance wavelengths are found at 590 nm, 600 nm, 620 nm, 640 nm, 660 nm, 700 nm, and 760 nm respectively.

Table 2. Comparison with other work

Ref.	Min peak loss (dB/cm)	Max WS (nm/RIU)	Max AS (1/RIU)	RI Range (RIU)	Resolution (RIU)
[15]	3.73 (x-polarized) 4.48 (y-polarized)	16,000	4,596 (x-polarized) 4,557 (y-polarized)	1.33–1.41	$6.25 \times 10^{-6}$
[14]	0.22 dB/cm (1.32) 2.87 dB/cm (1.4)	23,000	-	1.32–1.4	$4.34 \times 10^{-6}$
[16]	5.4 dB/cm	7,117	-	-	$1.4 \times 10^{-4}$
[17]	10.71 (x-polarized) 28.58 (y-polarized)	14,000	-1,212 (x-polarized) and -2,430 (y-polarized)	1.33–1.4	$7.14 \times 10^{-6}$
[18]	0.224 dB/cm	19,000	2,561	1.27–1.4	$5.26 \times 10^{-6}$
[29]	21	8,500	-335	1.34–1.37	$1.16 \times 10^{-5}$
[30]	0.79	34,000	1,170	1.32–1.41	$2.96 \times 10^{-5}$
[31]	0.00428	7,000	2,821.46	1.33–1.41	$5 \times 10^{-5}$
Proposed sensor	0.00117(x-polarized) 0.00307 (y-polarized)	6,000 (x-polarized) and y-polarized)	-385.4 (y-polarized) -373.4 (x-polarized)	1.32–1.38	$1.6 \times 10^{-7}$

### 3.3. Amplitude sensitivity

AS is a technique that can be used in optical sensing based on the difference from CL, mathematically the amplitude can be defined in (10):

$$AS(1/RIU) = -\frac{1}{\alpha(\lambda, n_a)} \frac{\partial \alpha(\lambda, n_a)}{\partial n_a} \quad (10)$$

AS is a technique that can be used in SPR-PCF based sensing. Max AS shift is accompanied by an increase in analyte RI. AS is obtained from (11) by making a difference of two adjacent CL, so that when it is varied with wavelength it can be seen in Figure 3(c) for x-polarized and Figure 3(d) for y-polarized. The maximum AS found were -385.4 1/RIU (y-polarized) and -373.4 1/RIU (x-polarized) and the RI of the analytes is 1.37 RIU. In another design, Nuzhat *et al.* [17] obtained the maximum AS in their design of -1212 (x-polarized) and -2430 (y-polarized). The results were obtained at analytes RI 1.39 RIU, meanwhile Islam *et al.* [15] obtained the maximum AS on the SPR-PCF sensor design of 4596 1/RIU (x-polarized) 4557 1/RIU (y-polarized) with an analyte RI of 1.4 RIU. Sultana *et al.* [18] obtained AS in their design 2561 1/RIU.

### 3.4. Sensor resolution

Sensor resolution is one of the most important performance parameters of a sensor, wide sensor resolution provides a wide range of wavelengths so that we can determine the appropriate wavelength range, sensor resolution can be calculated using (11):

$$R(RIU) = \frac{\Delta n_a \times \Delta \lambda_{min}}{\Delta \lambda_{peak}} \quad (11)$$

Where  $\Delta n_a$  represent the change in analyte RI,  $\Delta \lambda_{min}$  represent the minimum change in wavelength, and  $\Delta \lambda_{peak}$  is the change in the peak wavelength of the CL. In this sensor design the sensor resolution is obtained by  $1.6 \times 10^{-7}$  RIU (x-polarized and y-polarized).

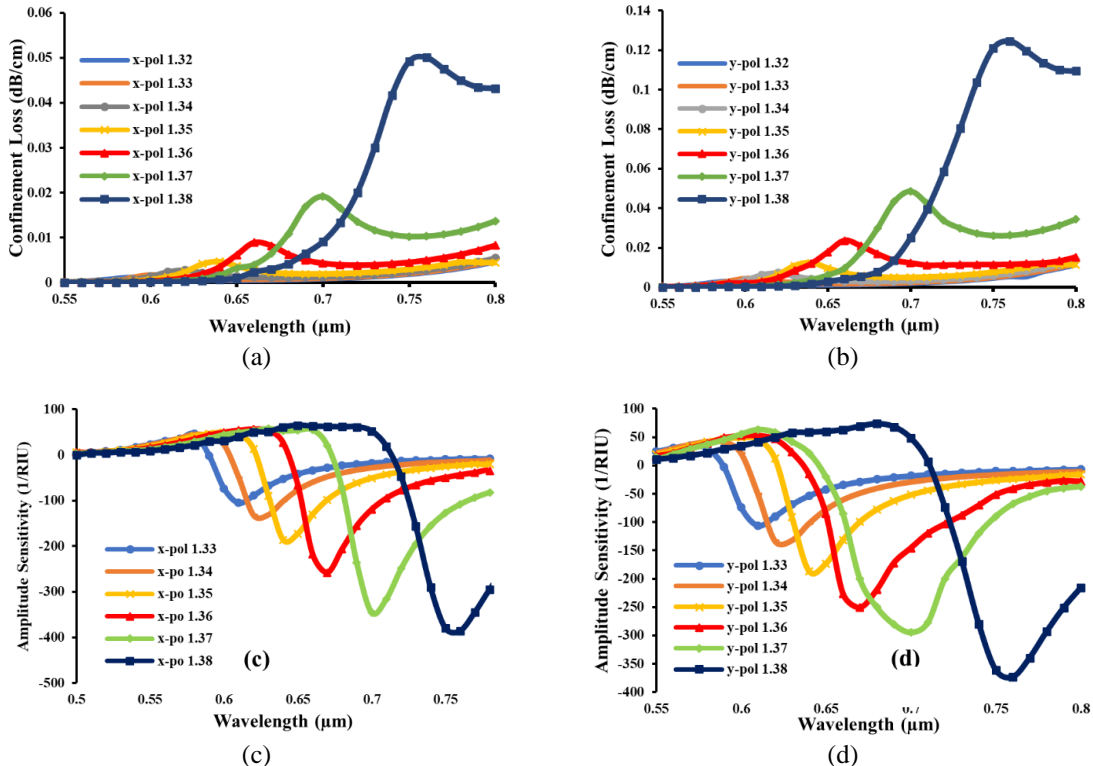


Figure 3. Performance of sensor; (a) CL at x-polarized, (b) CL at y-polarized, (c) AS at x-polarized, and (d) AS at y-polarized

### 3.5. The difference in confinement loss for each thickness of gold

In this case, we display the effect of Au thickness on CL (x-polarized and y-polarized). This can be seen in Figure 4. The Au thickness range in this section varies from 0.04 μm, 0.045 μm, and 0.05 μm, the RI of the specimen is 1.36 RIU, and the hole size in this case is 1.4 μm. The variation in CL is clearly related to gold thickness. The thicker the gold layer, the smaller the CL, but the thickness of the gold also affects the RW. For a gold thickness of 0.04 μm, the x- and y-polarized wavelengths are 650 nm and the CLs are 9.85 dB/cm and 3.9 dB/cm, respectively. The increase in thickness of 0.045 μm gold shows that the RW is at 660 nm with the CL of x-polarized and y-polarized respectively 8.4 dB/cm and 3.33 dB/cm. In this case there is a shift in wavelength of 10 nm. Furthermore, in the thickness of 0.05 μm thick gold the RW also shifts and is located at 670 nm with the CL on the x-polarized and y-polarized respectively being 6.62 dB/cm and 2.63 dB/cm. In other cases the effect of gold thickness did not show a shift in the RW as previously reported by researchers [32]–[35], but also in other designs showed no shift in the length of the resonance waveform along with an increase in the thickness of the gold layer [36].

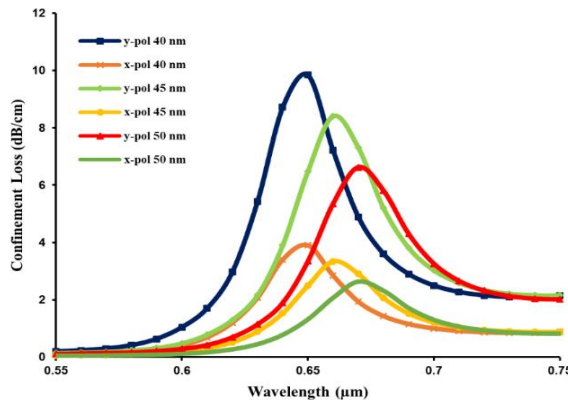


Figure 4. Effect of gold thickness on CL

### 3.6. Comparison with other sensor components

In this section we compare our work with previously reported work, the focus of the comparison is low-loss on sensor component, meanwhile max WS, max AS, RI range, and sensor resolution also shown as in Table 2. The sensor component has better performance than reported previously, our focus was to provide a sensor design with very low loss so that it can be applied to fiber optic. This components with a unique structure have a very low loss 0.00117 (x-polarized) and 0.00307 (y-polarized) compared to previous work, this is also supported by the sensor's ability to sense x-polarized and y-polarized, also the sensor has the ability to detect a RI from 1.32 RIU to 1.38 RIU.

## 4. CONCLUSION

This paper introduces a novel SPR-PCF sensor component designed for ease of fabrication, featuring twelve large holes surrounding the cladding, twelve medium-sized holes, and two small holes in close proximity to the core. Our numerical findings using FE demonstrate that the proposed sensor design exhibits an exceptional ultra-low loss of 0.00117 dB/cm (x-polarized) and 0.00307 dB/cm (y-polarized), surpassing previous reported losses. Additionally, the maximum WS and AS values are achieved at 6,000 nm/RIU (x-polarized and y-polarized), -385.4 1/RIU (y-polarized), and -373.4 1/RIU (x-polarized), respectively. Operating within a RI range of 1.32 to 1.38 RIU, this sensor demonstrates a remarkable resolution of  $1.6 \times 10^{-7}$  RIU for both x- and y-polarized measurements. Due to its high sensitivity, ultra-low loss, and dual-polarized propagation capabilities, this sensor component holds significant potential for remote detection of biochemical, biological, and biomedical analytes.

## ACKNOWLEDGEMENTS

We would like to thank the Ministry of Research, Technology, and Higher Education for providing funding support in this research through the LPPM with contract no. 11309/UN19.5.1.3/AL.04/2023. We would also like to thank the head of the Optoelectronic Laboratory at the University of Riau and the BRIN Physics Research Center for facilitating research activities.

## REFERENCES

- [1] A. K. Shakya, A. Ramola, S. Singh, and V. Van, "Design of an ultra-sensitive bimetallic anisotropic PCF SPR biosensor for liquid analytes sensing," *Optics Express*, vol. 30, no. 6, pp. 9233-9255, Mar. 2022, doi: 10.1364/OE.432263.
- [2] D. Irawan, K. Ramadhan, T. Saktioto, and A. Marwin, "An optimum design of high sensitivity PMMA-coated FBG sensor for temperature measurement," *TELKOMNIKA (Telecommunication Computing Electronics and Control)*, vol. 21, no. 2, pp. 382–389, Apr. 2023, doi: 10.12928/telkommika.v21i2.22746.
- [3] D. Irawan, K. Ramadhan, S. Saktioto, and A. Marwin, "Performance comparison of TOPAS chirped fiber Bragg grating sensor with Tanh and Gaussian apodization," *Indonesian Journal of Electrical Engineering and Computer Science*, vol. 26, no. 3, pp. 1477–1485, 2022, doi: 10.11591/ijeecs.v26.i3.pp1477-1485.
- [4] D. Irawan, K. Ramadhan, Saktioto, Fitmawati, Azhar, and A. Marwin, "Numerical investigation of photonic crystal fiber-based plasmonic material for alcohol concentration detection," *Materials Today: Proceedings*, Apr. 2023, pp. 299-302, doi: 10.1016/j.matpr.2023.03.285.
- [5] D. Irawan, K. Ramadhan, S. Saktioto, F. Fitmawati, D. Hanto, and B. Widjyatmoko, "Hexagonal two layers-photonics crystal fiber based on surface plasmon resonance with gold coating biosensor easy to fabricate," *Indonesian Journal of Electrical Engineering and Computer Science*, vol. 28, no. 1, pp. 146-154, Oct. 2022, doi: 10.11591/ijeecs.v28.i1.pp146-154.
- [6] H. Wu, C. Huang, R. Cui, and J. Zhou, "Simulation and Experiment Analysis of Temperature Field of Magnetic Suspension Support

Based on FBG," *Sensors*, vol. 22, no. 12, pp. 1-20, Jun. 2022, doi: 10.3390/s22124350.

[7] S. Gu *et al.*, "Simultaneous measurement of magnetic field and temperature based on photonic crystal fiber plasmonic sensor with dual-polarized modes," *Optik*, vol. 259, Jun. 2022, doi: 10.1016/j.ijleo.2022.169030.

[8] B. Han *et al.*, "Simultaneous measurement of temperature and strain based on dual SPR effect in PCF," *Optics & Laser Technology*, vol. 113, pp. 46-51, May 2019, doi: 10.1016/j.optlastec.2018.12.010.

[9] B. Li, F. Zhang, X. Yan, X. Zhang, F. Wang, and T. Cheng, "An Optical Fiber-Based Surface Plasmon Resonance Sensor for Simultaneous Measurement of Temperature and Magnetic Field Intensity," *IEEE Transactions on Instrumentation and Measurement*, vol. 71, pp. 1-7, 2022, doi: 10.1109/TIM.2021.3134307.

[10] W. Liu *et al.*, "A square-lattice D-shaped photonic crystal fiber sensor based on SPR to detect analytes with large refractive indexes," *Physica E: Low-dimensional Systems and Nanostructures*, vol. 138, Apr. 2022, doi: 10.1016/j.physe.2021.115106.

[11] K. M. M. Rahman, M. S. Alam, and M. A. Islam, "Highly Sensitive Surface Plasmon Resonance Refractive Index Multi-Channel Sensor for Multi-Analyte Sensing," *IEEE Sensors Journal*, vol. 21, no. 24, pp. 27422-27432, Dec. 2021, doi: 10.1109/JSEN.2021.3126624.

[12] A. Yasli and H. Ademgil, "Effect of plasmonic materials on photonic crystal fiber based surface plasmon resonance sensors," *Modern Physics Letters B*, vol. 33, no. 13, pp. 1-15, May 2019, doi: 10.1142/S0217984919501574.

[13] S. Sen, M. Abdullah-Al-Shafi, A. S. Sikder, M. S. Hossain, and M. M. Azad, "Zeonex based decagonal photonic crystal fiber (D-PCF) in the terahertz (THz) band for chemical sensing applications," *Sensing and Bio-Sensing Research*, vol. 31, pp. 1-7, 2021, doi: 10.1016/j.sbsr.2020.100393.

[14] M. Al Mahfuz, M. A. Hossain, E. Haque, N. H. Hai, Y. Namihira, and F. Ahmed, "A Bimetallic-Coated, Low Propagation Loss, Photonic Crystal Fiber Based Plasmonic Refractive Index Sensor," *Sensors*, vol. 19, no. 17, pp. 1-12, Sep. 2019, doi: 10.3390/s19173794.

[15] M. R. Islam *et al.*, "Design and analysis of birefringent SPR based PCF biosensor with ultra-high sensitivity and low loss," *Optik*, vol. 221, pp. 1-14, Nov. 2020, doi: 10.1016/j.ijleo.2020.165311.

[16] L. Yang *et al.*, "Detection of kerosene adulteration in automobile fuel by a low-loss surface plasmon resonance (SPR) chemical sensor," *Analytical Methods*, vol. 14, no. 22, pp. 2153-2160, 2022, doi: 10.1039/D2AY00508E.

[17] S. Nuzhat, S. Sultana, F. Bin Hassan, S. K. Biswas, M. Das Gupta, and H. Talukder, "Dual scaled approach SPR-based PCF RI sensor with ultra-low loss," *Journal of Physics: Conference Series*, vol. 2070, no. 1, pp. 1-12, Nov. 2021, doi: 10.1088/1742-6596/2070/1/012109.

[18] S. Sultana, M. F. Bin Hassan, H. Talukder, and S. K. Biswas, "Optimization and Sensitivity Analysis of a Single Core Low Loss PCF Sensor," in *2021 5th International Conference on Electrical Engineering and Information Communication Technology (ICEEICT)*, Nov. 2021, pp. 1-6, doi: 10.1109/ICEEICT53905.2021.9667880.

[19] D. M. Mattox, "Physical vapor deposition (PVD) processes," *Metal Finishing*, vol. 98, no. 1, pp. 410-423, Jan. 2000, doi: 10.1016/S0026-0576(00)80350-5.

[20] A. Csaki *et al.*, "Nanoparticle Layer Deposition for Plasmonic Tuning of Microstructured Optical Fibers," *Small*, vol. 6, no. 22, pp. 2584-2589, Nov. 2010, doi: 10.1002/smll.201001071.

[21] B. S. Lim, A. Rahtu, and R. G. Gordon, "Atomic layer deposition of transition metals," *Nature Materials*, vol. 2, no. 11, pp. 749-754, Nov. 2003, doi: 10.1038/nmat1000.

[22] B. Brixner, "Refractive-Index Interpolation for Fused Silica\*," *Journal of the Optical Society of America*, vol. 57, no. 5, pp. 674-676, May 1967, doi: 10.1364/JOSA.57.000674.

[23] H. S. Sehmi, W. Langbein, and E. A. Muljarov, "Optimizing the Drude-Lorentz model for material permittivity: Method, program, and examples for gold, silver, and copper," *Physical Review B*, vol. 95, no. 11, pp. 1-8, Mar. 2017, doi: 10.1103/PhysRevB.95.115444.

[24] M. R. Hasan *et al.*, "Spiral Photonic Crystal Fiber-Based Dual-Polarized Surface Plasmon Resonance Biosensor," *IEEE Sensors Journal*, vol. 18, no. 1, pp. 133-140, Jan. 2018, doi: 10.1109/JSEN.2017.2769720.

[25] M. B. Hossain *et al.*, "Numerical development of high performance quasi D-shape PCF-SPR biosensor: An external sensing approach employing gold," *Results in Physics*, vol. 18, pp. 1-21, Sep. 2020, doi: 10.1016/j.rinp.2020.103281.

[26] S. Singh and Y. K. Prajapati, "Dual-polarized ultrahigh sensitive gold/MoS<sub>2</sub>/graphene based D-shaped PCF refractive index sensor in visible to near-IR region," *Optical and Quantum Electronics*, vol. 52, no. 1, pp. 1-15, Jan. 2020, doi: 10.1007/s11082-019-2122-3.

[27] C. Dou, X. Jing, S. Li, Q. Liu, and J. Bian, "A Photonic Crystal Fiber Polarized Filter at 1.55  $\mu$ m Based on Surface Plasmon Resonance," *Plasmonics*, vol. 11, no. 4, pp. 1163-1168, Aug. 2016, doi: 10.1007/s11468-015-0155-4.

[28] A. Zuhayer, M. Abd-Elnaby, S. H. Ahammad, M. M. A. Eid, V. Sorathiya, and A. N. Z. Rashed, "A Gold-Plated Twin Core D-Formed Photonic Crystal Fiber (PCF) for Ultrahigh Sensitive Applications Based on Surface Plasmon Resonance (SPR) Approach," *Plasmonics*, vol. 17, no. 5, pp. 2089-2101, Oct. 2022, doi: 10.1007/s11468-022-01700-0.

[29] S. Asaduzzaman and K. Ahmed, "Investigation of ultra-low loss surface plasmon resonance-based PCF for biosensing application," *Results in Physics*, vol. 11, pp. 358-361, Dec. 2018, doi: 10.1016/j.rinp.2018.09.026.

[30] M. S. Islam, M. R. Islam, J. Sultana, A. Dinovitzer, B. W.-H. Ng, and D. Abbott, "Exposed-core localized surface plasmon resonance biosensor," *Journal of the Optical Society of America B*, vol. 36, no. 8, pp. 2306-2311, Aug. 2019, doi: 10.1364/JOSAB.36.002306.

[31] S. R. Tahhan and R. M. Taha, "Mercedes Benz logo based plasmon resonance PCF sensor," *Sensing and Bio-Sensing Research*, vol. 35, pp. 1-9, Feb. 2022, doi: 10.1016/j.sbsr.2021.100468.

[32] Z. Yin *et al.*, "A broadband SPR dual-channel sensor based on a PCF coated with sodium-silver for refractive index and temperature measurement," *Results in Physics*, vol. 41, pp. 1-9, Oct. 2022, doi: 10.1016/j.rinp.2022.105943.

[33] M. Al Mahfuz *et al.*, "Highly sensitive photonic crystal fiber plasmonic biosensor: Design and analysis," *Optical Materials*, vol. 90, pp. 315-321, Apr. 2019, doi: 10.1016/j.optmat.2019.02.012.

[34] F. Wang, C. Liu, Z. Sun, T. Sun, B. Liu, and P. K. Chu, "A Highly Sensitive SPR Sensors Based on Two Parallel PCFs for Low Refractive Index Detection," *IEEE Photonics Journal*, vol. 10, no. 4, pp. 1-10, Aug. 2018, doi: 10.1109/JPHOT.2018.2856273.

[35] D. Irawan, K. Ramadhan, T. Saktioto, F. Fitmawati, D. Hanto, and B. Widiyatmoko, "High-Performance of Star-Photonic Crystal Fiber Based on Surface Plasmon Resonance Sensor," *Indian Journal of Pure & Applied Physics*, vol. 60, pp. 727-733, Aug. 2022, doi: 10.56042/ijpap.v6i09.64411.

[36] D. F. Santos, A. Guerreiro, and J. M. Baptista, "SPR optimization using metamaterials in a D-type PCF refractive index sensor," *Optical Fiber Technology*, vol. 33, pp. 83-88, Jan. 2017, doi: 10.1016/j.yofte.2016.11.010.

## BIOGRAPHIES OF AUTHORS



**Dr. Dedi Irawan M.Sc.**     is a lecturer at Laboratory of PMIPA, Department of Physics Education, Universitas Riau, Pekanbaru, Indonesia. He works on basic and advanced photonics. Focus research on the development of optoelectronic component for communication and sensor application. He obtained Ph.D. degree in 2013 at Universiti Teknologi Malaysia. He can be contacted at email: [dedi.irawan@lecturer.unri.ac.id](mailto:dedi.irawan@lecturer.unri.ac.id).



**Khaikal Ramadhan S.Si.**     was a student at the University of Riau in 2017 and has finished studying Physics at the Universitas Riau with a B.Sc. degree in 2021. Now he is master student at Institute Teknologi Bandung Indonesia. He can be contacted at email: [khaikal.ramadhan4946@student.unri.ac.id](mailto:khaikal.ramadhan4946@student.unri.ac.id).



**Prof. Dr. Saktioto S.Si., M. Phil.**     is a senior lecturer at Department of Physics, Faculty of Mathematics and Natural Sciences (FMIPA), Universitas Riau, Pekanbaru, Indonesia. His research fields are plasma photonics, optoelectronics component, and metamaterial. He can be contacted at email: [Saktioto@yahoo.com](mailto:Saktioto@yahoo.com).



**Prof. Dr. Fitmawati M.Si.**     is an active lecturer in Department of Biology, Faculty of Mathematics and Natural Sciences (FMIPA), Universitas Riau. She is head Department of Biological Science and active doing research related to cancer phenomenon. She can be contacted at email: [fitmawati2008@yahoo.com](mailto:fitmawati2008@yahoo.com).



**Dwi Hanto Ph.D.**     is a researcher at the BRIN Puspitek Fisika. He is currently doing research about the development of optoelectronic component, such as FBG, circulator, and also doing experimental research using LIDAR. He can be contacted at email: [dwi.hanto.fisika@gmail.com](mailto:dwi.hanto.fisika@gmail.com)



**Dr. Bambang Widjyatmoko M.Eng.** is a senior researcher at BRIN Puspitek Fisika. His focus research is fiber bragg grating, and various FBG sensor application was developed in laboratory scale. He can be contacted at email: Widjyatmokobambang@gmail.com.



**Azwir Marwin** was a student at the FMIPA University of Riau in 2019. He is physics student which is doing research related to biochemical sensor application: theoretical and experimental development and focus on the biochemical sensing. He can be contacted at email: azwir.marwin4971@student.unri.ac.id.



**Assoc Prof. Azhar S.Pd., M.T.** is a lecturer at the Department of Physics Education FMIPA UNRI. He actively doing research in implementation of optical physics as learning media for physics students and also for senior high school students. He can be contacted at email: Azhar@lecturer.unri.ac.id.